



**HAL**  
open science

# Adsorption of Quinolone Antibiotics to Goethite under Seawater Conditions: Application of a Surface Complexation Model

Wei Cheng, Elaheh Lotfi Kalahroodi, Remi Marsac, Khalil Hanna

► **To cite this version:**

Wei Cheng, Elaheh Lotfi Kalahroodi, Remi Marsac, Khalil Hanna. Adsorption of Quinolone Antibiotics to Goethite under Seawater Conditions: Application of a Surface Complexation Model. *Environmental Science and Technology*, 2019, 53 (3), pp.1130-1138. 10.1021/acs.est.8b04853 . hal-01964933

**HAL Id: hal-01964933**

**<https://hal.science/hal-01964933>**

Submitted on 24 Dec 2018

**HAL** is a multi-disciplinary open access archive for the deposit and dissemination of scientific research documents, whether they are published or not. The documents may come from teaching and research institutions in France or abroad, or from public or private research centers.

L'archive ouverte pluridisciplinaire **HAL**, est destinée au dépôt et à la diffusion de documents scientifiques de niveau recherche, publiés ou non, émanant des établissements d'enseignement et de recherche français ou étrangers, des laboratoires publics ou privés.

## Adsorption of Quinolone Antibiotics to Goethite under Seawater Conditions: Application of a Surface Complexation Model

Wei Cheng, Elaheh Lotfi Kalahroodi, Rémi Marsac, and Khalil Hanna

*Environ. Sci. Technol.*, **Just Accepted Manuscript** • DOI: 10.1021/acs.est.8b04853 • Publication Date (Web): 21 Dec 2018

Downloaded from <http://pubs.acs.org> on December 24, 2018

### Just Accepted

“Just Accepted” manuscripts have been peer-reviewed and accepted for publication. They are posted online prior to technical editing, formatting for publication and author proofing. The American Chemical Society provides “Just Accepted” as a service to the research community to expedite the dissemination of scientific material as soon as possible after acceptance. “Just Accepted” manuscripts appear in full in PDF format accompanied by an HTML abstract. “Just Accepted” manuscripts have been fully peer reviewed, but should not be considered the official version of record. They are citable by the Digital Object Identifier (DOI®). “Just Accepted” is an optional service offered to authors. Therefore, the “Just Accepted” Web site may not include all articles that will be published in the journal. After a manuscript is technically edited and formatted, it will be removed from the “Just Accepted” Web site and published as an ASAP article. Note that technical editing may introduce minor changes to the manuscript text and/or graphics which could affect content, and all legal disclaimers and ethical guidelines that apply to the journal pertain. ACS cannot be held responsible for errors or consequences arising from the use of information contained in these “Just Accepted” manuscripts.

1     **Adsorption of Quinolone Antibiotics to Goethite under Seawater**  
2             **Conditions: Application of a Surface Complexation Model**

3             Wei Cheng <sup>a</sup>, Elaheh Lotfi Kalahroodi <sup>b</sup>, Rémi Marsac <sup>b</sup>, Khalil Hanna <sup>\*a</sup>

4

5     <sup>a</sup>Univ Rennes, Ecole Nationale Supérieure de Chimie de Rennes, CNRS, ISCR – UMR6226,

6                             F-35000 Rennes, France

7     <sup>b</sup>Univ Rennes, CNRS, Géosciences Rennes - UMR 6118, F-35000 Rennes, France

8

9             \*Corresponding author: Tel.: +33 2 23 23 80 27; fax: +33 2 23 23 81 20.

10                             E-mail address: khalil.hanna@ensc-rennes.fr (K. Hanna)

11

12

13                             A revised manuscript submitted to *ES&T*

14

December, 2018

15

17 **ABSTRACT**

18

19 The assessment of antibiotics mobility under seawater conditions has been rarely studied,  
20 since an accurate description of such multicomponent systems is quite challenging. In this  
21 study, the adsorption of a widely used quinolone antibiotic in aquaculture, Oxolinic acid (OA),  
22 to a synthetic goethite ( $\alpha$ -FeOOH) was examined in presence of major (e.g.  $\text{Mg}^{2+}$ ,  $\text{SO}_4^{2-}$ ) and  
23 trace (e.g.  $\text{Cu}^{2+}$ ) ions naturally occurring in seawater. The OA adsorption can be successfully  
24 predicted using a charge distribution multi-site complexation model (CD-MUSIC) coupled  
25 with the three plane model (TPM). This modeling approach allowed a quantification of the  
26 competitive and synergetic effects of different ions in seawater over a large range of  
27 environmentally relevant conditions. In addition, the transport of OA in flow-through columns  
28 can be well predicted through coupling hydrodynamic parameters and surface complexation  
29 constants obtained under seawater conditions. These results may have strong implications for  
30 assessment and prediction of the fate of quinolones in sediment/seawater interface systems.

31

## 32 1. INTRODUCTION

33 Quinolone antibiotics, broad-spectra antimicrobial agents, are widely used in the treatment  
34 and prevention of bacterial diseases of fish.<sup>1,2</sup> Among them, Oxolinic Acid (OA) is commonly  
35 used as a prophylactic, or, as a chemotherapy agent.<sup>1,2</sup> Due to its frequent use<sup>3</sup>, high residual  
36 levels of OA were detected in aquatic systems, *i.e.* in concentration ranging from 2.50 ppm in  
37 fresh or saline surface waters to 426 ppm in pond sediments.<sup>4-6</sup> Because of the rapid growth  
38 of aquaculture in different countries, impacts of antibiotics overuse on the environment are  
39 becoming of big concern.<sup>7</sup> Therefore, it is necessary to investigate the transport and mobility  
40 of quinolones in marine ecosystems, in order to accurately assess their ecological impacts.

41 In marine environments, mineral particles present in suspension or in sediments are able  
42 to bind quinolones, which may affect their mobility and bioavailability in water.<sup>8</sup> Among  
43 these reactive mineral surfaces, goethite ( $\alpha$ -FeOOH) is the most thermodynamically stable  
44 iron oxyhydroxide mineral and the most common diagenetic iron oxyhydroxide in both  
45 marine and lake sediments.<sup>9</sup> Recently, goethite has been shown to strongly sorb OA across a  
46 wide range of salinity (10–1000 mM NaCl) including seawater-like one.<sup>8</sup> However, cations  
47 and anions existing in seawater environments naturally or due to anthropogenic activities,  
48 could affect the mobility of OA in marine ecosystems. This may proceed through (i)  
49 complexation with divalent transition metals in aqueous solution<sup>10,11</sup> and (ii) competitive or  
50 cooperative binding to mineral surfaces.<sup>12-16</sup>

51 Despite the widespread use of quinolones in fish farming, the effect of cations and anions  
52 found in seawater on their solubility and adsorption behavior to suspended mineral particles  
53 or mineral sediments has received little attention. In this study, interactions of OA with  
54 goethite in presence of two major ions (e.g.  $Mg^{2+}$ ,  $SO_4^{2-}$ ) and one trace cation ( $Cu^{2+}$  used as a  
55 model trace metal in seawater) have been studied under a wide range of ion concentrations  
56 and pH values. Possible antagonistic or synergetic effects on OA adsorption have also been

57 investigated in presence of mixture of  $Mg^{2+}$ ,  $SO_4^{2-}$  and  $Cu^{2+}$ , and in synthetic seawater. The  
58 ability of the three plane model (TPM) to predict competitive or cooperative interactions on  
59 goethite surfaces has been evaluated under a wide range of pH (4-10). Finally, this  
60 thermodynamic adsorption model was used to predict the breakthrough behavior of OA in a  
61 goethite-packed column under water-saturated conditions.

62 Given the complexity of the seawater matrix where a wide array of cations and anions exist, a  
63 quantitative framework for assessing competitive or synergetic interactions both under static  
64 and hydrodynamic conditions is quite challenging. For the first time, TPM combined with the  
65 charge distribution-multisite complexation (CD-MUSIC) model is successfully applied to  
66 predict binding mechanisms of contaminants on mineral particles in the presence of major and  
67 trace ions of seawater, and then the reactive transport under flow-through conditions.

68

## 69 **2. MATERIALS AND METHODS**

70 **2.1. Materials.** All reagents were purchased from Sigma-Aldrich and used without further  
71 purification. All solutions were prepared with ultrapure water. An OA (purity >99%) stock  
72 solution was prepared by dissolving 30 mg (115  $\mu$ moles) OA in 20 mL of 1 M NaOH, then  
73 diluted to 1 L with ultrapure water.

74 **2.2. Synthesis and Characterization of Goethite Particles.** Goethite was synthesized as  
75 described in previous studies.<sup>8,17</sup> Briefly, 400 mL of a 2.5 mol L<sup>-1</sup> sodium hydroxide solution  
76 was mixed with 500 mL of a 0.5 mol L<sup>-1</sup> ferric nitrate solution ( $Fe(NO_3)_3 \cdot 9H_2O$ ) at a fixed  
77 rate of 1 mL min<sup>-1</sup> with stirring under nitrogen atmosphere. The obtained hydroxide slurry  
78 was aged at 60 °C for 72 hours in an oven. The precipitate obtained was then dialyzed  
79 (Spectra/Por membrane 2) against Milli-Q water. The water was changed every day until its  
80 conductivity was close to 0  $\mu$ S cm<sup>-1</sup>. The suspensions were stored in polypropylene containers  
81 at 4 °C for further use. The purity of goethite was confirmed by X-ray diffraction (XRD) and

82 the B.E.T. specific surface area of the synthetic goethite was  $80 \pm 1 \text{ m}^2 \text{ g}^{-1}$  and the point of zero  
83 charge (PZC) of goethite, determined under  $\text{N}_2$  atmosphere at 298 K in 0.01, 0.1 and 1 M  
84 NaCl solutions by the potentiometric titration method, was pH 9.1. Goethite coated sand  
85 (GCS) was prepared by coating goethite onto sieved Fontainebleau quartz sand (100–150  $\mu\text{m}$ )  
86 as previously detailed.<sup>18</sup>

87 **2.3. Batch adsorption experiments.** Because pH measurements will be affected by high  
88 background electrolyte solutions, the pH electrode was calibrated to measure the molarity of  
89 the proton ( $-\log [\text{H}^+]$ , noted as pHc) using solutions of known  $[\text{H}^+]$  ( $10^{-5}$ – $10^{-2}$  M) in 480 mM  
90 NaCl, and the results are provided in this form in this study. The procedure was repeated in  
91 presence of other ions ( $\text{Mg}^{2+}$ ,  $\text{SO}_4^{2-}$ ,  $\text{Cu}^{2+}$ ).

92 OA solubility experiments (undersaturation direction) were conducted by suspending solid  
93 OA ( $\sim 3$ – $5 \text{ mg}$ ) in 10 mL of 480 mM NaCl with different concentrations of  $\text{Mg}^{2+}$  and  
94 adjusting pHc from 4 to 8 using HCl and NaOH. The suspensions were equilibrated for 24 h  
95 (a sufficient time for assessing aqueous drug solubility<sup>19</sup>), after that the supernatants were  
96 filtered (0.2  $\mu\text{m}$ ) and OA concentrations were measured with high pressure liquid-  
97 chromatography coupled with UV detection (HPLC-UV).

98 All batch experiments were carried out under  $\text{N}_{2(\text{g})}$  atmosphere to avoid effects of  
99 carbonates and bicarbonates on the adsorption of OA onto goethite. Batch adsorption  
100 experiments were carried out in 15 mL polyethylene tubes at a total volume of 10 mL solution  
101 with 10  $\mu\text{M}$  OA, 480 mM NaCl and 50  $\text{m}^2 \text{ L}^{-1}$  goethite.  $\text{MgCl}_2$  (10 and 50 mM),  $\text{CuCl}_2$  (10, 50  
102 and 100  $\mu\text{M}$ ) and/or  $\text{Na}_2\text{SO}_4$  (1, 10 and 29 mM) were added to the solutions in order to study  
103 the effects (and combined effects) of  $\text{Mg}^{2+}$ ,  $\text{SO}_4^{2-}$  and/or  $\text{Cu}^{2+}$  on OA adsorption. The solution  
104 compositions of each experiment are listed in [Table S1](#). The pHc was then adjusted to the  
105 desired value ( $4 < \text{pHc} < 10$ ) with HCl or NaOH solutions. The tubes were sealed by caps and  
106 then shaken continuously on a platform shaker at 200 rpm and 25 °C. After equilibrating for

107 24 h, pHc was measured again before filtration (0.2  $\mu\text{m}$ ) and OA was analyzed by HPLC-UV.  
108 Desorption tests (pHc = 11) were carried out under various experimental conditions to check  
109 the mass balance of OA (Table S2).

110 To study OA adsorption in conditions closer to the marine environment, an artificial  
111 seawater was synthesized according to the method of Kester et al.<sup>20</sup> Table S3 shows the major  
112 elements present in the synthetic seawater. However, batch experiments were conducted in  
113 absence of  $\text{NaHCO}_3$  in order to avoid the potential complication of competing carbonate  
114 adsorption.

115 Aqueous OA concentrations were determined using a high performance liquid  
116 chromatography (Waters 600 Controller) equipped with a UV detector (Waters 2489) and a  
117 reversed-phase C18 column (250 mm $\times$ 4.6 mm i.d., 5  $\mu\text{m}$ ). The mobile phase (1 mL  $\text{min}^{-1}$ )  
118 was a mixture of acetonitrile/water (60:40 v/v) contained 0.1% formic acid. The detector was  
119 set to 259 nm for OA. Concentrations of  $\text{Cu}^{2+}$  and  $\text{Mg}^{2+}$  were analyzed by Varian AA140  
120 Atomic Absorption Spectrometer. The sulfate concentration was measured by DIONEX IX  
121 Chromatograph DX-120.

122 **2.4. Flow-through column experiments.** Breakthrough column experiments were  
123 conducted according to Hanna et al.<sup>18,21</sup> Briefly, 15 g of dry GCS was packed into glass  
124 chromatographic columns of 1.6 cm internal diameter to give a porous bed length of 4.7 cm.  
125 After packing to a uniform bulk density ( $1.59 \pm 0.05\text{g cm}^{-3}$ ), the column was wetted upward  
126 with a synthetic seawater solution at a constant flow rate. Once the column was water  
127 saturated, the flow characteristics of the porous bed were determined by a nonreactive tracer  
128 experiment, as previously described.<sup>18,21</sup> The classical convection dispersion equation (CDE)  
129 was applied to describe the 1D transport of a non-reactive solute (bromide) under steady-state  
130 water flow. The fitting result provided estimations of the volumetric water content ( $\theta$ ) and  
131 dispersion coefficient (D) that characterize of flow homogeneity. The dispersivity ( $\lambda$ ) was

132 calculated according to  $\lambda = D\theta/q$ , neglecting the molecular diffusion. At a flow rate of 0.5 mL  
133  $\text{min}^{-1}$ , the Darcy velocity ( $q$ ) was 0.25  $\text{cm min}^{-1}$ , the volumetric water content  $\theta$  was found  
134 equal to 0.42  $\text{cm}^3 \text{cm}^{-3}$ , water velocity  $v = 0.59 \text{ cm min}^{-1}$ ,  $D = 0.009 \text{ cm}^2 \text{min}^{-1}$  and  $\lambda$  was 151  
135  $\mu\text{m}$  within order of magnitude of particle size of the used sand. The Péclet number ( $Pe = vL/D$ ,  
136  $L$  is total column length) in the column was higher than 300, indicating the predominance of a  
137 convective regime. Similarly, these parameters were also calculated for 0.1  $\text{mL min}^{-1}$  as flow  
138 rate.

139 Two different conditions of inflow solution, with or without carbonates, were tested. In  
140 both tests, a mixture of 10  $\mu\text{M}$  OA and 10  $\mu\text{M}$   $\text{Cu}^{2+}$  was injected in the column at a constant  
141 flow rate (0.5  $\text{mL min}^{-1}$  or 0.1  $\text{mL min}^{-1}$ ). OA concentrations in the collected fractions were  
142 measured by HPLC/UV.

143 **2.5. Surface Complexation Modeling.** Predictions of OA adsorption to goethite were  
144 made using the multisite complexation (MUSIC) model approach.<sup>22</sup> The geochemical  
145 speciation code PHREEQC (version 2)<sup>23</sup> was used for surface complexation calculations. The  
146 charge of the goethite/water interface was treated by using the three plane model (TPM).  
147 Charges of the adsorbates were distributed among the 0 ( $\text{H}^+$ , metal-bonded OA), 1 (hydrogen-  
148 bonded OA), and 2 ( $\text{Na}^+$ ,  $\text{Cl}^-$ ) planes of the TPM. Although not required for OA binding to  
149 goethite,<sup>8</sup> a charge distribution (CD) term was used in the present work to describe the  
150 adsorption of other ions on goethite. Singly ( $\equiv\text{FeOH}^{-0.5}$ ), doubly ( $\equiv\text{Fe}_2\text{OH}$ ) and triply ( $\equiv\text{Fe}_3\text{O}^{-0.5}$   
151  $^{0.5}$  and  $\equiv\text{Fe}_3\text{OH}^{+0.5}$ ) coordinated oxygens outcrop the goethite surface, depending on the  
152 crystal face. A simplified 1-pK surface charging model, neglecting the contributions of  
153 doubly- and part of the triply-coordinated oxygens, was used. The reactive site density in this  
154 model are detailed in SI:<sup>8</sup>  $[\equiv\text{FeOH}^{-0.5}] = 3.12 \text{ sites nm}^{-2}$  and  $[\equiv\text{Fe}_3\text{O}^{-0.5}] = 3.12 \text{ sites nm}^{-2}$  on  
155 (001)/(101) planes (90% of the surface area), and  $[\equiv\text{FeOH}^{-0.5}] = 7.4 \text{ sites nm}^{-2}$  on (021) plane  
156 (10% of the surface area). The protonation constants of these groups are set to that of the

157 pH<sub>pzc</sub> (1-pK approach of MUSIC model). Equilibrium constants of the formation of all  
 158 surface species are reported in Table 1. PhreePlot<sup>24</sup> was used to determine parameters for OA  
 159 sorption to goethite. Parameters describing goethite surface (e.g. pK<sub>a</sub>, capacitances) and OA-  
 160 goethite binding were taken from our previous work.<sup>8</sup>

161 PHREEQC can use various equations to account for the non-ideality of aqueous solutions.  
 162 In this study, a modified version of the Debye-Hückel equation, called WATEQ, was used  
 163 with the “minteq.v4” database provided with PHREEQC:

$$164 \log \gamma_i = -\frac{Az_i^2\sqrt{I}}{1 + Ba_i^0\sqrt{I}} + b_i I \quad (1)$$

165 Where  $\gamma_i$  and  $z_i$  are, respectively, the activity coefficient and the charge of the ion  $i$ , A and B  
 166 are temperature dependent parameters (A=0.5095 and B=0.3284×10<sup>8</sup> at 25 °C),  $a_i^0$  and  $b_i$  are  
 167 fitted ion-specific parameters. This equation is valid up to ionic strength (I) values of about 2  
 168 M in dominantly chloride solutions.<sup>25</sup> Because these parameters are missing for OA aqueous  
 169 species,  $Ba_i^0$  was systematically set to 1.5 (i.e.,  $a_i^0 = 4.57 \times 10^{-8}$ ), as commonly adopted in the  
 170 specific ion interaction theory (SIT<sup>26</sup>), a more advance model than the WATEQ equation. All  
 171 necessary parameters are available in the “minteq.v4” database except for OA species.  $b_{OA^-} =$   
 172  $b_{OAH} = 0$  was used, as in our previous study.<sup>8</sup>  $b_{OAMg^+}$  was fitted using Phreeplot and OA  
 173 solubility data in presence of Mg<sup>2+</sup>.  $b_{OACu^+}$  and  $b_{OACa^+}$  were assumed equal to  $b_{OAMg^+}$ .

174 All studied ions were included in the calculations, and PHREEQC calculates the ionic  
 175 strength according to the solution composition. As shown below, surface complexations of  
 176 almost all ions were taken into account except Br<sup>-</sup> and H<sub>3</sub>BO<sub>3</sub>. Br<sup>-</sup> is expected to behave  
 177 similarly to Cl<sup>-</sup>, but is about 660 times less abundant than Cl<sup>-</sup> in seawater. To our knowledge,  
 178 no CD-MUSIC parameters are available to describe H<sub>3</sub>BO<sub>3</sub> sorption to goethite. Therefore,  
 179 the adsorption of Br<sup>-</sup> and H<sub>3</sub>BO<sub>3</sub> was neglected as a first approach.

180 Precipitations of  $\text{Mg}(\text{OH})_{2(s)}$ ,  $\text{Ca}(\text{OH})_{2(s)}$  and  $\text{Cu}(\text{OH})_{2(s)}$  were taken into account in the  
 181 calculations. Only  $\text{Mg}(\text{OH})_{2(s)}$  could form under alkaline conditions, which had little effect on  
 182 the adsorption behavior and interpretations.

183 PhreePlot<sup>24</sup> was used when parameter adjustment was required. It also provides a  
 184 statistical uncertainty for the estimated parameters (see Table 1). Parameters were fitted  
 185 separately from independent datasets in simple (binary) systems, and then kept constant for  
 186 simulations in more complex systems. For instance,  $b_{\text{OAMg}^+}$  was determined using OA  
 187 solubility data in presence of  $\text{Mg}^{2+}$  and kept constant afterwards. Goethite-OA and goethite-  
 188  $\text{Mg}^{2+}$  surface complexation constants were determined in previous studies dedicated to the  
 189 corresponding binary system.<sup>8,27</sup> Then, simulations were made (with no parameter adjustment)  
 190 in the ternary goethite- $\text{Mg}^{2+}$ -OA system. This step-by-step procedure was used in all systems,  
 191 hence limiting the uncertainties on newly adjusted model parameters.

192

### 193 3. RESULTS AND DISCUSSION

#### 194 3.1. OA solubility and binding to goethite in 480 mM NaCl

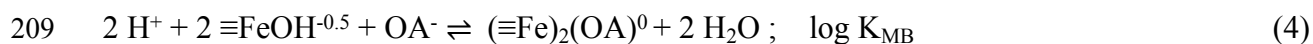
195 The OA solubility was first calculated with PHREEQC using the acidity constant ( $K_a$ )  
 196 value from the IUPAC stability constant database and the solubility constant ( $K_s$ ) previously  
 197 determined (with  $b_{\text{OA}^-} = b_{\text{OAH}} = 0$ ):<sup>8</sup>



200 The experimental solubility values are very close to the calculated ones (Figure S-1a). In  
 201 480 mM NaCl, OA solubility increased with pH increasing.

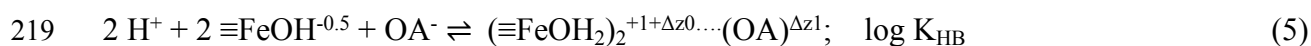
202 OA adsorption shows typical anion adsorption character on goethite surfaces, i.e.  
 203 adsorption reaches a maximum value at acidic to circumneutral pH and then decreases with  
 204 increasing pH (Figure S-1b).<sup>8</sup> According to previous infrared spectroscopic investigations,<sup>8</sup>

205 OA binds to goethite predominantly through a metal-bonded (MB) complexes with surface Fe  
 206 sites and a strong hydrogen-bonded (HB) complexes (surface hydration shared ion pair) with  
 207 surface hydroxo groups. MB surface complex formed at the goethite (101)/(001) and (210)  
 208 planes involving OA keto group and one oxygen of the carboxylate group:



210  
 211 Only singly coordinated ( $\equiv\text{FeOH}^{-0.5}$ ) surface sites are considered to be involved in the  
 212 reaction given the propensity for ligand exchange of these sites. Eq.4 does not denote the  
 213 number of Fe(III) octahedra in a complex but only the number of  $\equiv\text{FeOH}^{-0.5}$  sites that may or  
 214 may not be of the same Fe(III) octahedron.<sup>28</sup> Ideally, the steric constraints at the dominant  
 215 (101)/(001) planes should promote bridging between two Fe atoms separated by 3 Å from one  
 216 another,<sup>29</sup> while at the (210) plane, two  $\equiv\text{FeOH}^{-0.5}$  should be located on the same Fe(III)  
 217 octahedron, hence our preference for modeling OA binding as a 1:2 OA/ $\equiv\text{FeOH}^{-0.5}$  species.

218 Hydrogen-bonded (HB) complexation with singly  $\equiv\text{FeOH}^{-0.5}$  sites was also proposed:



220  
 221 In our previous work,<sup>8</sup> the CD approach was not used and OA negative charge was placed  
 222 at the 1-plane ( $\Delta z_0 = 0$ ;  $\Delta z_1 = -1$ ). In general, within the CD-MUSIC framework, 0.2 bond  
 223 valence unit can be assigned to each H-bond.<sup>30</sup> Because OA binds to goethite surface via two  
 224 H-bonds (one with each of two adjacent  $\equiv\text{FeOH}_2^{+0.5}$  sites), a CD value of 0.4 was used ( $\Delta z_0 =$   
 225  $-0.4$ ;  $\Delta z_1 = -0.6$ ). In fact, this had minor effect on the prediction of OA-goethite binding and  
 226 as shown in [Figure S-1b](#), the model predicts well OA adsorption onto goethite at high salt  
 227 concentration (i.e. 480 mM NaCl).

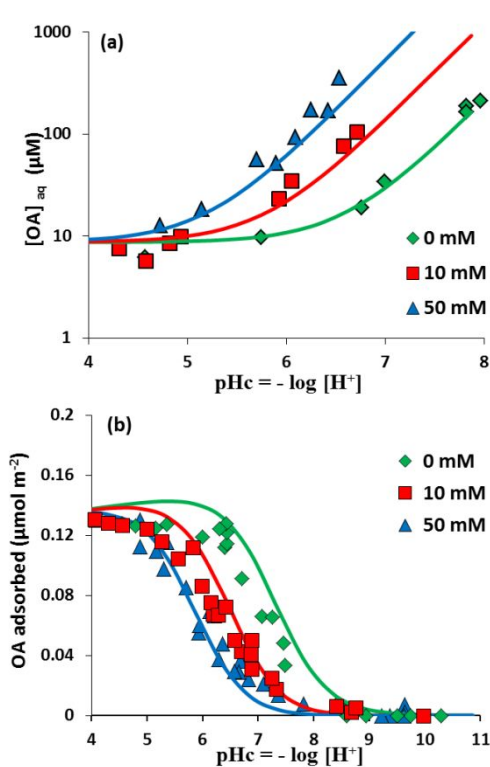
### 228 3.2. Effect of $\text{Mg}^{2+}$ on OA solubility and binding to goethite

229 The equilibrium constant of the formation of the aqueous  $\text{OAMg}^+$  complex has previously  
 230 been reported at  $I = 0.1 \text{ M}$ :<sup>10</sup>



232 In the present study, Mg-OA complexation in 480 mM NaCl was investigated via  
233 measurements of OA solubility at different  $MgCl_2$  concentrations (Figure 1a). As expected,  
234 OA apparent solubility increased with increasing  $[Mg^{2+}]$  due to the formation of  $OAMg^+$   
235 aqueous complex. The formation constant of  $OAMg^+$  was determined at infinite dilution ( $\log$   
236  $K_{OA-Mg} = 3.51$ ) using previously reported constant at  $I = 0.1$  M.<sup>10</sup> An accurate prediction of  
237 OA apparent solubility in presence of  $Mg^{2+}$  (Figure 1a) can be achieved by adjusting  $b_{OAMg^+}$   
238 ( $= 0.5$ ) using Phreeplot.

239 Figure 1b shows OA adsorption to goethite in 480 mM NaCl at different  $Mg^{2+}$   
240 concentrations (0, 10 and 50 mM). The presence of  $Mg^{2+}$  decreased OA adsorption to goethite  
241 at all pH values and shifted the sorption edge to lower pH values. As previously reported,<sup>12,13</sup>  
242 the effect of  $Mg^{2+}$  could be explained by the formation of an aqueous complex and/or  
243 competition effects towards surface sites.  $Mg^{2+}$  adsorption to goethite is weak and could not  
244 be accurately determined at a  $Mg^{2+}$  concentration as high as that used in the present work.  
245 This is also in agreement with a previous report,<sup>30</sup> where  $Mg^{2+}$  adsorption became only  
246 detectable at  $pH > 8$  and at lower  $[Mg^{2+}]$  ( $\leq 0.4$  mM) in 0.1 M  $NaNO_3$ . At such pH value,  
247 there is almost no OA adsorption in our experiments, ruling out possible competitive effect  
248 with  $Mg^{2+}$ . Accounting for  $OAMg^+$  formation in the OA adsorption model agreed with our  
249 experimental values. Including  $Mg^{2+}$ -goethite surface complexation<sup>30</sup> did not affect the  
250 simulations, thereby confirming the predominant contribution of the aqueous complex  
251  $OAMg^+$  (Figure 1b).



252

253 **Figure 1.** (a) OA solubility in 480 mM NaCl at different MgCl<sub>2</sub> concentrations. (b) OA (10254 μM) adsorption to goethite (50 m<sup>2</sup> L<sup>-1</sup>) in 480 mM NaCl versus pHc at different MgCl<sub>2</sub>

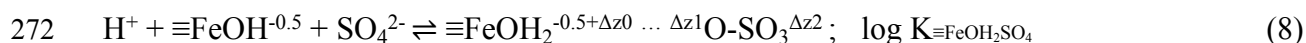
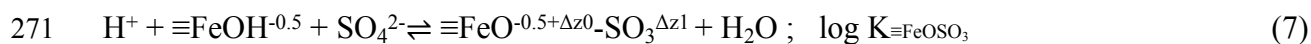
255 concentrations after 24h reaction time. Lines are modeling results.

256 **3.3. Effect of SO<sub>4</sub><sup>2-</sup> on OA binding to goethite**

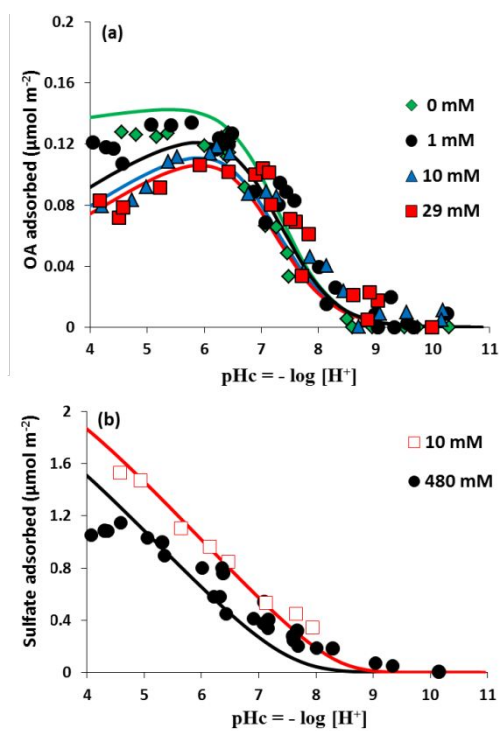
257 **Figure 2a** shows OA adsorption to goethite at different SO<sub>4</sub><sup>2-</sup> concentrations (0, 1, 10 and  
258 29 mM). At 1 mM of SO<sub>4</sub><sup>2-</sup>, there is almost no effect on OA adsorption. For larger [SO<sub>4</sub><sup>2-</sup>],  
259 OA adsorption is only decreased at low pH values (pHc < 6.5), with no significant influence  
260 at higher pH (**Figure 2a**).

261 To maximize sensitivity to residual sulfate concentration determination, SO<sub>4</sub><sup>2-</sup> adsorption  
262 was only determined at the lowest [SO<sub>4</sub><sup>2-</sup>] (i.e. 1 mM). Because ionic chromatography  
263 measurements of aqueous [SO<sub>4</sub><sup>2-</sup>] are subjected to large error due to interferences caused by  
264 Cl<sup>-</sup>, adsorption experiment was investigated at both 10 and 480 mM NaCl concentrations  
265 (**Figure 2b**). As typically observed for anion adsorption to iron oxides, sulfate adsorption  
266 decreased with increasing pH.<sup>31-34</sup> According to several vibrational spectroscopy

267 studies,<sup>32,35,36</sup> both inner-sphere complexes and outer-sphere complexes are supposed to form  
 268 between  $\text{SO}_4^{2-}$  and the goethite surface. Therefore, a monodentate MB complex (eq.7) and a  
 269 monodentate HB surface (eq.8) complex can be proposed to describe the adsorption data as  
 270 following:<sup>37</sup>



273 The charge of  $\text{SO}_4^{2-}$  is distributed over the 0- and 1-plane for the MB complex, and  
 274 between the 1- and 2-plane for the HB complex. By fitting only the surface complexation  
 275 constants in the present investigation (see Table 1), our model satisfactorily described sulfate  
 276 adsorption versus pH and ionic strength (Figure 2b). By keeping these new parameters  
 277 constants, the model successfully predicted competitive effect of sulfate on OA at pH<7, but  
 278 underestimated OA adsorption at higher pH values (Figure 2a). This experimental and  
 279 modeling data confirm the sulfate competition for OA adsorption at low pH values.



280  
 281 **Figure 2.** (a) OA removal from solution for  $[\text{OA}]_{\text{tot}} = 10 \mu\text{M}$  on  $50 \text{ m}^2 \text{ L}^{-1}$  goethite in 480 mM

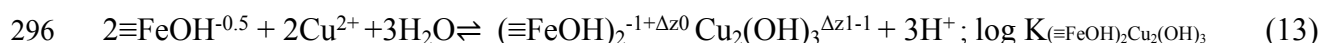
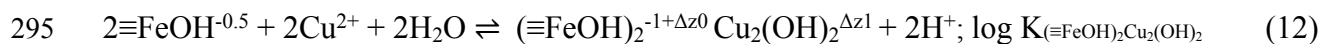
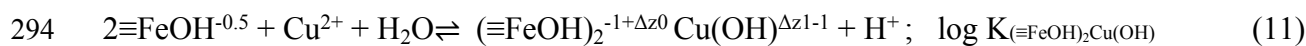
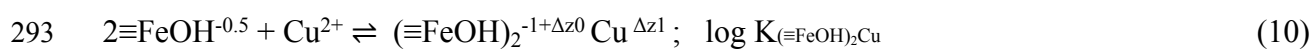
282 NaCl versus pHc at different Na<sub>2</sub>SO<sub>4</sub> concentrations and (b) Sulfate removal for [Na<sub>2</sub>SO<sub>4</sub>] = 1  
 283 mM and [OA]<sub>tot</sub> = 10 μM at two NaCl concentrations on 50 m<sup>2</sup> L<sup>-1</sup> goethite versus pHc after  
 284 24h reaction time. Lines are modeling results.

### 285 3.4. Effect of Cu<sup>2+</sup> on OA binding to goethite

286 The equilibrium constant of the formation of the aqueous OACu<sup>+</sup> complex has been  
 287 reported to be much larger than that of OAMg<sup>+</sup> complex at I = 0.1 M:<sup>10</sup>



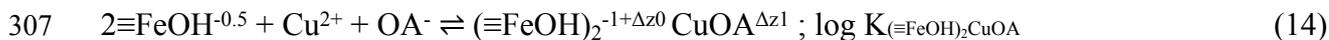
289 By using the WATEQ equation and setting  $b_{\text{OACu}^+} = b_{\text{OAMg}^+} = 0.5$ , log K<sub>OA-Cu</sub> was  
 290 found equal to 6.61. Figure 3a shows that copper adsorption to goethite increases with pH, for  
 291 the three tested concentrations (10, 50 and 100 μM). Based on previous report,<sup>38</sup> four  
 292 equations can be proposed to describe the binding of Cu<sup>2+</sup> to goethite:



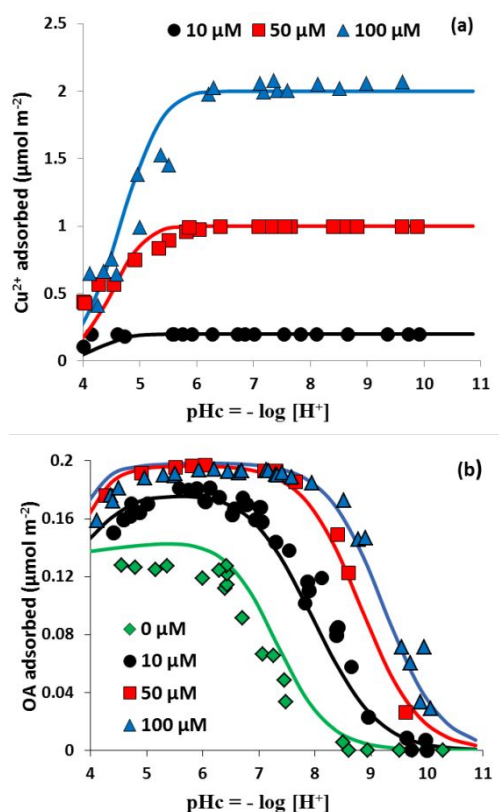
297 Using this model, our Cu<sup>2+</sup> uptake data in 480 mM NaCl can be well predicted by only  
 298 adjusting log K<sub>(≡FeOH)<sub>2</sub>Cu(OH)</sub> (eq.11), while keeping all other parameters equal to literature  
 299 values.<sup>31</sup>

300 The presence of Cu<sup>2+</sup> significantly enhanced OA adsorption at all pH values, whereas OA  
 301 adsorption increased with increasing Cu<sup>2+</sup> concentration (Figure 3b). As previously  
 302 reported,<sup>14,38-41</sup> the formation of a surface-Cu<sup>2+</sup>-organic ligand ternary complex may explain  
 303 the enhancement in OA adsorption. Indeed, Cu<sup>2+</sup> may act as a bridge ion to form a six-  
 304 member ring with the carboxylic and carbonyl groups.<sup>39</sup> Accordingly, accounting for a ternary

305 goethite-Cu<sup>2+</sup>-OA complex (eq.14) allows an accurate prediction of OA binding to goethite in  
 306 presence of Cu<sup>2+</sup> (Figure 3b):



308 This phenomenon is favored by (i) the great OA-Cu<sup>+</sup> aqueous complexation and (ii) the  
 309 overlapping in pH-edges of OA and Cu<sup>2+</sup>.<sup>42</sup> Note that all other parameters were kept constant  
 310 while fitting log K<sub>(≡FeOH)<sub>2</sub>CuOA</sub>.



311  
 312 **Figure 3.** (a) Cu<sup>2+</sup> and (b) OA removal from solutions for [OA]<sub>tot</sub> = 10 μM on 50 m<sup>2</sup> L<sup>-1</sup>  
 313 goethite in 480 mM NaCl versus pHc at different CuCl<sub>2</sub> concentrations after 24h reaction time.

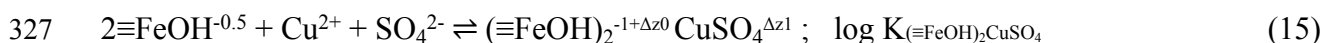
314 Lines are modeling results.

### 315 3.5. OA-goethite binding in presence of Mg<sup>2+</sup>, SO<sub>4</sub><sup>2-</sup> and Cu<sup>2+</sup>

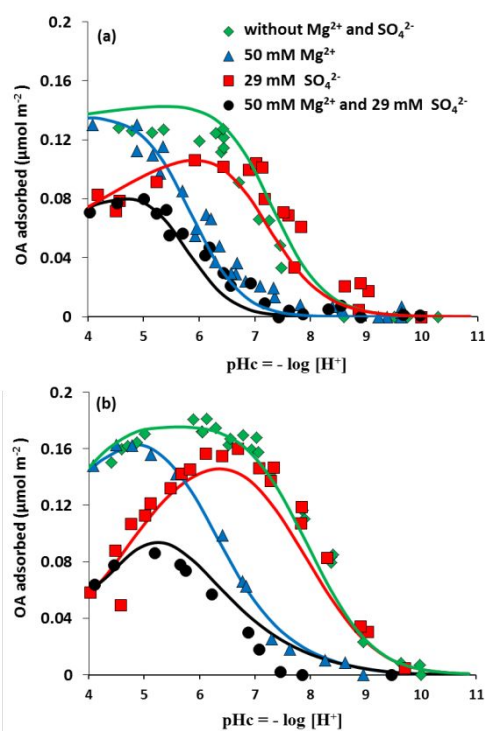
316 As shown in Figure 4a, OA-goethite pH-edge in presence of mixture of Mg<sup>2+</sup> and SO<sub>4</sub><sup>2-</sup>  
 317 exhibits the previously observed features, i.e. Mg<sup>2+</sup> decreased OA adsorption and shifted  
 318 sorption edge to lower pH, while SO<sub>4</sub><sup>2-</sup> decreased only significantly OA adsorption at low pH

319 values. Interestingly, our SCM has well predicted the experimental data without further  
 320 parameter adjustment.

321 As expected, the presence of 10  $\mu\text{M}$   $\text{Cu}^{2+}$  increased OA-goethite binding even in presence  
 322 of 50 mM  $\text{Mg}^{2+}$  and/or 29 mM  $\text{SO}_4^{2-}$  (Figure 4b). However, the model overestimated OA  
 323 (Figure S-2a) and underestimated  $\text{Cu}^{2+}$  (Figure S-2b) adsorption to goethite at low pH,  
 324 respectively. As an attempt to improve the description of our experimental data, we include a  
 325 ternary surface goethite-Cu-sulfate complex in the present model (applying the same fitting  
 326 procedure as for the goethite-Cu-OA complex), as previously suggested:<sup>43</sup>



328 We assumed that  $\text{Cu}^{2+}$  charge is located at the 0 plane and charge distribution of  $\text{SO}_4^{2-}$  is  
 329 similar to that of MB complex in eq. 7 (i.e. -0.5 charge at the 0-plane, -1.5 at the 1-plane). This  
 330 equation has permitted to enhance Cu-goethite binding and limit the goethite-Cu-OA surface  
 331 complex formation, thereby considerably improving the prediction of both  $\text{Cu}^{2+}$  (Figure S-2c)  
 332 and OA adsorption to goethite (Figure 4b).



333

334 **Figure 4.** OA removal from solutions for  $[OA]_{\text{tot}} = 10 \mu\text{M}$  on  $50 \text{ m}^2 \text{ L}^{-1}$  goethite in 480 mM  
335 NaCl versus pHc at 50 mM  $\text{MgCl}_2$  and /or 29 mM  $\text{Na}_2\text{SO}_4$  after 24h reaction time in presence  
336 of (a)  $0 \mu\text{M}$   $\text{CuCl}_2$  (b)  $10 \mu\text{M}$   $\text{CuCl}_2$ . Lines are modeling results. Same legends for (a) and (b).

337 It is worth noting that no further parameter adjustment was made in the following  
338 sections, which aim at testing the capability of the present model to predict OA adsorption  
339 and transport under conditions closer to marine environments.

340

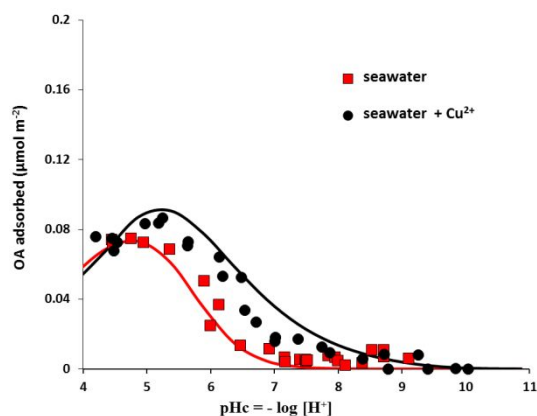
### 341 3.6. OA adsorption in synthetic seawater

342 OA adsorption edges in synthetic seawater is similar to that obtained in presence of 50  
343 mM  $\text{MgCl}_2$  and 29 mM  $\text{Na}_2\text{SO}_4$  at 480 mM NaCl (Figure S-3), suggesting that  $\text{Mg}^{2+}$  and  
344  $\text{SO}_4^{2-}$  are the most influencing ions in synthetic seawater investigated here. Other ions such as  
345  $\text{F}^-$ ,  $\text{Br}^-$ ,  $\text{BO}_3^{3-}$  and  $\text{Ca}^{2+}$  have no significant impact on OA adsorption due to their lower  
346 concentrations in synthetic seawater. When the aqueous complexation of  $\text{Ca}^{2+}$  and OA:<sup>10</sup>



348 and surface complexation of  $\text{Ca}^{2+}$  to goethite<sup>30</sup> and  $\text{F}^-$  to goethite<sup>44</sup> are introduced in the  
349 present model (see more details in Table 1), only a slight difference in the predicted OA-  
350 goethite binding is observed, as compared to that simulated in presence of only  $\text{Mg}^{2+}$  and  
351  $\text{SO}_4^{2-}$  (Figure S-3).

352 The presence of  $\text{Cu}^{2+}$  in synthetic seawater overrides partially the negative effects of major  
353 ions and, thus, increased OA adsorption (Figure 5).  $\text{Cu}^{2+}$  adsorption to goethite in seawater or  
354 in presence of 50 mM  $\text{MgCl}_2$  and 29 mM  $\text{Na}_2\text{SO}_4$  at 480 mM NaCl did not exhibit a  
355 significant difference (Figure S-4). The model predicted quite well OA and  $\text{Cu}^{2+}$  adsorption to  
356 goethite in seawater without further parameter adjustment (Figure 5 and Figure S-4).



357

358 **Figure 5.** OA removal from synthetic seawater for  $[OA]_{\text{tot}} = 10 \mu\text{M}$  on  $50 \text{ m}^2 \text{ L}^{-1}$  goethite  
359 versus pHc with or without  $10 \mu\text{M}$   $\text{CuCl}_2$  after 24h reaction time. Lines are modeling results.

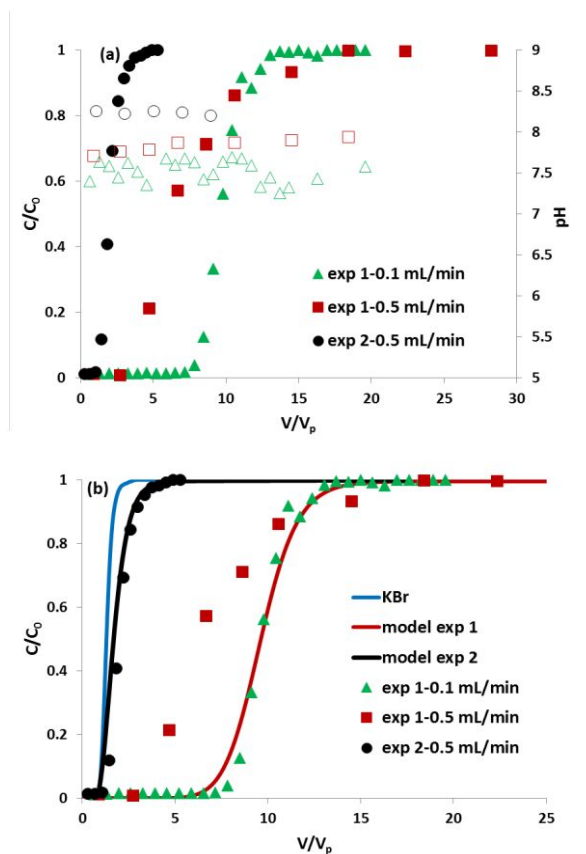
### 360 3.7. OA transport under seawater conditions

361 In order to assess the OA binding to goethite surfaces under flow-through conditions,  
362 dynamic experiments were carried out using goethite-coated sand (GCS) packed column.  
363 Column saturation has been made using synthetic seawater to emulate water-saturated marine  
364 sediments.

365 In a first experiment, the column was injected with  $10 \mu\text{M}$  OA and  $10 \mu\text{M}$   $\text{Cu}^{2+}$  dissolved  
366 in synthetic seawater as used in batch experiments (Table S-3 without carbonates), at a water  
367 velocity of  $0.5 \text{ mL min}^{-1}$ . The pH of inflow solution lied at  $7.4 \pm 0.1$ , and then slightly  
368 increased in the column system (exp1-  $0.5 \text{ mL min}^{-1}$  in Figure 6a). The total adsorbed amount  
369 at complete OA breakthrough ( $\sim 0.03 \mu\text{mol m}^{-2}$ ) is close to that expected from the batch  
370 experiments (Figure 5). However, the predicted breakthrough using batch-derived parameters  
371 overestimated OA sorption in the column system and showed a large retardation (see Figure  
372 6b). The fast OA transportation at  $0.5 \text{ mL min}^{-1}$  could possibly be related to the lack of local  
373 geochemical equilibrium in the column, as previously observed in numerous reports.<sup>21,45–48</sup>  
374 The steepness of the BTC of OA as compared to that of bromide (i.e. the BTC of OA is more  
375 tilted than that of the tracer) as well as the short tail observed in the BTC of OA suggests that  
376 sorption kinetic limitations might take place in the column. In order to test this possibility, an

377 additional flow-through experiment was performed at a lower flow rate ( $0.1 \text{ mL min}^{-1}$ ) using  
378 the same conditions of exp1 (i.e.  $10 \text{ }\mu\text{M OA}$ ,  $10 \text{ }\mu\text{M Cu}^{2+}$ ,  $\text{pH}_{\text{in}} 7.4 \pm 0.1$ ) (Figure 6a). The  
379 experimental breakthrough curve becomes more sigmoidal in shape at  $0.1 \text{ mL min}^{-1}$  and  
380 shows no extended tailing. A higher residence time promotes more OA retention in the  
381 column and pushes the breakthrough point to  $\sim 7$  injected pore volumes (PV) compared to  $\sim 3$   
382 PV at  $0.5 \text{ mL min}^{-1}$ , proving that the sorption equilibrium was not reached within the time  
383 scale of the column experiment. Interestingly, very good agreement between the experimental  
384 and calculated breakthrough curves is observed at  $0.1 \text{ mL min}^{-1}$  (Figure 6b).

385 In a second experiment,  $10 \text{ }\mu\text{M OA}$  and  $10 \text{ }\mu\text{M Cu}^{2+}$  dissolved in synthetic seawater  
386 containing  $2.3 \text{ mM NaHCO}_3$  (full composition displayed in Table S-3), closer to the real  
387 seawater at  $\text{pH } 8.2$ ,<sup>20</sup> was injected at  $0.5 \text{ mL min}^{-1}$ . Because of a higher pH value (Figure 6a),  
388 lower adsorption and faster breakthrough were obtained, which is in agreement with the batch  
389 data. The breakthrough point of OA lies at  $1.5 \text{ PV}$ , while total breakthrough occurs at  $\sim 4 \text{ PV}$ .  
390 The predicted breakthrough using batch-derived parameters describes quite well OA transport  
391 in the column under salt water conditions and  $\text{pH } 8.2$  (Figure 6b). Carbonate-goethite binding  
392 was accounted using parameters derived by Rahnemaie et al.<sup>49</sup> (Figure S-5). This data  
393 confirms that transport modeling using hydrodynamic parameters defined by the tracer  
394 breakthrough experiment and the surface complexation parameters can be successfully used to  
395 predict adsorption of quinolone antibiotics onto goethite under seawater conditions and at two  
396 environmentally relevant pH values ( $7.4$  and  $8.2$ ).



397

398 **Figure 6.** (a) Experimental breakthrough curves of OA and pH at two inflow conditions. exp  
399 1: injection of 10  $\mu\text{M}$  OA and 10  $\mu\text{M}$   $\text{Cu}^{2+}$  in synthetic seawater. exp 2: injection of 10  $\mu\text{M}$   
400 OA and 10  $\mu\text{M}$   $\text{Cu}^{2+}$  in synthetic seawater containing carbonates as for the real seawater (see  
401 Table S-3) (b) Calculated BTC of OA and tracer (bromide).

402

#### 403 4. ENVIRONMENTAL IMPLICATIONS

404 We have notably demonstrated that TPM can be successfully used to predict adsorption of  
405 quinolone antibiotics onto goethite over a large range of environmentally relevant conditions  
406 and both under static and flow-through conditions. In addition, the reactive transport of OA  
407 can be well simulated through coupling hydrodynamic parameters and surface complexation  
408 constants. This modeling approach allowed a quantification of the effects of different ions  
409 naturally present in seawater on OA retention. Although  $\text{SO}_4^{2-}$  is known as a strong  
410 competitor for anions, its effect on OA-goethite binding at seawater relevant pH was found

411 almost negligible. Other less abundant ions such as  $F^-$ ,  $Br^-$ ,  $BO_3^{3-}$  and  $Ca^{2+}$  did not exhibit a  
412 significant impact. However, at seawater relevant concentrations,  $Mg^{2+}$  was found to strongly  
413 reduce OA-goethite binding via the formation of aqueous complex with OA. Furthermore,  
414 trace metals (e.g.  $Cu^{2+}$  used here as a model metal) naturally occurring in seawater could  
415 strongly increase OA binding by forming a ternary metal-ligand surface complex. It is worth  
416 noting that the presence of natural organic matter in marine and/or estuary ecosystems could  
417 also alter the binding mechanism of quinolones onto minerals and then their mobility in  
418 marine ecosystems. This last point stresses the need for a more detailed study to assess the  
419 application of surface complexation model (SCM) in real seawater containing natural organic  
420 matter. These findings may have strong implications in the prediction of transport of  
421 quinolones antibiotics, and thus assessment of ecological impacts of aquaculture induced  
422 pollution in marine systems.

423

#### 424 **SUPPORTING INFORMATION**

425 Thermodynamic calculations of OA solubility and sorption in 480 Mm NaCl; modeling tests  
426 of OA and/or  $Cu^{2+}$  adsorption under different conditions; simulations of carbonate binding to  
427 goethite.

#### 428 **ACKNOWLEDGMENTS**

429 This work was supported by Région Bretagne (K.H). We gratefully acknowledge the Chinese  
430 Scholarship Council of PR China for providing financial support for Wei Cheng to stay at the  
431 ENSCR.

432

#### 433 **REFERENCES**

- 434 (1) Samuelsen, O. B.; Ervik, A.; Pursell, L.; Smith, P. Single-Dose Pharmacokinetic Study of  
435 Oxolinic Acid and Vetoquinol, an Oxolinic Acid Ester, in Atlantic Salmon (*Salmosalar*) Held  
436 in Seawater and in Vitro Antibacterial Activity against *Aeromonassalmonicida*. *Aquaculture*  
437 **2000**, *187* (3), 213–224. [https://doi.org/10.1016/S0044-8486\(00\)00315-X](https://doi.org/10.1016/S0044-8486(00)00315-X).

- 438 (2) Samuelsen, O. B.; Bergh, Ø.; Ervik, A. A Single-Dose Pharmacokinetic Study of Oxolinic Acid  
439 and Vetoquinol, an Oxolinic Acid Ester, in Cod, *Gadus Morhua* L., Held in Sea Water at 8 °C  
440 and in Vitro Antibacterial Activity of Oxolinic Acid against *Vibrio Anguillarum* Strains  
441 Isolated from Diseased Cod. *J. Fish Dis.* **2003**, *26* (6), 339–347. [https://doi.org/10.1046/j.1365-](https://doi.org/10.1046/j.1365-2761.2003.00466.x)  
442 [2761.2003.00466.x](https://doi.org/10.1046/j.1365-2761.2003.00466.x).
- 443 (3) Picó, Y.; Andreu, V. Fluoroquinolones in Soil—Risks and Challenges. *Anal. Bioanal. Chem.*  
444 **2007**, *387* (4), 1287–1299. <https://doi.org/10.1007/s00216-006-0843-1>.
- 445 (4) Rigos, G.; Nengas, I.; Alexis, M.; Troisi, G. M. Potential Drug (Oxytetracycline and Oxolinic  
446 Acid) Pollution from Mediterranean Sparid Fish Farms. *Aquat. Toxicol.* **2004**, *69* (3), 281–288.  
447 <https://doi.org/10.1016/j.aquatox.2004.05.009>.
- 448 (5) Le, T. X.; Munekage, Y. Residues of Selected Antibiotics in Water and Mud from Shrimp  
449 Ponds in Mangrove Areas in Viet Nam. *Mar. Pollut. Bull.* **2004**, *49* (11), 922–929.  
450 <https://doi.org/10.1016/j.marpolbul.2004.06.016>.
- 451 (6) Samuelsen, O. B. Pharmacokinetics of Quinolones in Fish: A Review. *Aquaculture* **2006**, *255*  
452 (1–4), 55–75. <https://doi.org/10.1016/j.aquaculture.2005.12.008>.
- 453 (7) Cabello, F. C. Heavy Use of Prophylactic Antibiotics in Aquaculture: A Growing Problem for  
454 Human and Animal Health and for the Environment. *Environ. Microbiol.* **2006**, *8* (7), 1137–  
455 1144. <https://doi.org/10.1111/j.1462-2920.2006.01054.x>.
- 456 (8) Marsac, R.; Martin, S.; Boily, J.-F.; Hanna, K. Oxolinic Acid Binding at Goethite and  
457 Akaganéite Surfaces: Experimental Study and Modeling. *Environ. Sci. Technol.* **2016**, *50* (2),  
458 660–668. <https://doi.org/10.1021/acs.est.5b04940>.
- 459 (9) Liu, H.; Chen, T.; Frost, R. L. An Overview of the Role of Goethite Surfaces in the  
460 Environment. *Chemosphere* **2014**, *103*, 1–11.  
461 <https://doi.org/10.1016/j.chemosphere.2013.11.065>.
- 462 (10) Timmers, K.; Sternglanz, R. Ionization and Divalent Cation Dissociation Constants of  
463 Nalidixic and Oxolinic Acids. *Bioinorg. Chem.* **1978**, *9* (2), 145–155.
- 464 (11) Park, H. R.; Jeong, G. Y.; Lee, H. C.; Lee, J. G.; Baek, G. M. Ionization and Divalent Cation  
465 Complexation of Quinolone Antibiotics in Aqueous Solution. *Bull. Korean Chem. Soc.* **2000**,  
466 *21* (9), 849–854.
- 467 (12) Kong, X.; Feng, S.; Zhang, X.; Li, Y. Effects of Bile Salts and Divalent Cations on the  
468 Adsorption of Norfloxacin by Agricultural Soils. *J. Environ. Sci.* **2014**, *26* (4), 846–854.  
469 [https://doi.org/10.1016/S1001-0742\(13\)60480-5](https://doi.org/10.1016/S1001-0742(13)60480-5).
- 470 (13) Balistriero, L. S.; Murray, J. W. The Influence of the Major Ions of Seawater on the Adsorption  
471 of Simple Organic Acids by Goethite. *Geochim. Cosmochim. Acta* **1987**, *51* (5), 1151–1160.
- 472 (14) Pei, Z.; Shan, X.-Q.; Kong, J.; Wen, B.; Owens, G. Coadsorption of Ciprofloxacin and Cu(II)  
473 on Montmorillonite and Kaolinite as Affected by Solution PH. *Environ. Sci. Technol.* **2010**, *44*  
474 (3), 915–920. <https://doi.org/10.1021/es902902c>.
- 475 (15) Figueroa, R. A.; Leonard, A.; MacKay, A. A. Modeling Tetracycline Antibiotic Sorption to  
476 Clays. *Environ. Sci. Technol.* **2004**, *38* (2), 476–483. <https://doi.org/10.1021/es0342087>.
- 477 (16) Wang, Y.-J.; Jia, D.-A.; Sun, R.-J.; Zhu, H.-W.; Zhou, D.-M. Adsorption and Cosorption of  
478 Tetracycline and Copper(II) on Montmorillonite as Affected by Solution PH. *Environ. Sci.*  
479 *Technol.* **2008**, *42* (9), 3254–3259. <https://doi.org/10.1021/es702641a>.
- 480 (17) Gaboriaud, F.; Ehrhardt, J.-J. Effects of Different Crystal Faces on the Surface Charge of  
481 Colloidal Goethite ( $\alpha$ -FeOOH) Particles: An Experimental and Modeling Study. *Geochim.*  
482 *Cosmochim. Acta* **2003**, *67* (5), 967–983.
- 483 (18) Hanna, K.; Martin, S.; Quilès, F.; Boily, J.-F. Sorption of Phthalic Acid at Goethite Surfaces  
484 under Flow-Through Conditions. *Langmuir* **2014**, *30* (23), 6800–6807.  
485 <https://doi.org/10.1021/la4049715>.
- 486 (19) Ross, D. L.; Riley, C. M. Aqueous Solubilities of Some Various Substituted Quinolone  
487 Antimicrobials. *Int. J. Pharm.* **1990**, *63* (3), 237–250. [https://doi.org/10.1016/0378-](https://doi.org/10.1016/0378-5173(90)90130-V)  
488 [5173\(90\)90130-V](https://doi.org/10.1016/0378-5173(90)90130-V).
- 489 (20) Kester, D. R.; Duedall, I. W.; Connors, D. N.; Pytkowicz, R. M. Preparation of Artificial  
490 Seawater. *Limnol. Oceanogr.* **1967**, *12* (1), 176–179.  
491 <https://doi.org/10.4319/lo.1967.12.1.0176>.

- 492 (21) Hanna, K.; Boily, J.-F. Sorption of Two Naphthoic Acids to Goethite Surface under Flow  
493 through Conditions. *Environ. Sci. Technol.* **2010**, *44* (23), 8863–8869.  
494 <https://doi.org/10.1021/es102903n>.
- 495 (22) Hiemstra, T.; Van Riemsdijk, W. H. A Surface Structural Approach to Ion Adsorption: The  
496 Charge Distribution (CD) Model. *J. Colloid Interface Sci.* **1996**, *179* (2), 488–508.
- 497 (23) Parkhurst, D. L.; Appelo, C. A. J. User's Guide to PHREEQC (Version 2): A Computer  
498 Program for Speciation, Batch-Reaction, One-Dimensional Transport, and Inverse  
499 Geochemical Calculations. **1999**.
- 500 (24) Kinniburgh, D.; Cooper, D. PhreePlot: Creating graphical output with PHREEQC  
501 <http://www.phreeplot.org/PhreePlot.pdf> (accessed Aug 29, 2018).
- 502 (25) Parkhurst, D. L. Ion-Association Models and Mean Activity Coefficients of Various Salts. In  
503 *Chemical Modeling of Aqueous Systems II*; ACS Symposium Series; American Chemical  
504 Society, 1990; Vol. 416, pp 30–43. <https://doi.org/10.1021/bk-1990-0416.ch003>.
- 505 (26) Grenthe, I.; Plyasunov, A. V.; Spahiu, K. Estimations of Medium Effects on Thermodynamic  
506 Data. *Model. Aquat. Chem.* **1997**, 325–426.
- 507 (27) Stachowicz, M.; Hiemstra, T.; van Riemsdijk, W. H. Multi-Competitive Interaction of As(III)  
508 and As(V) Oxyanions with Ca<sup>2+</sup>, Mg<sup>2+</sup>, PO<sub>3</sub><sup>4-</sup>, and CO<sub>2</sub><sup>3-</sup> Ions on Goethite. *J. Colloid  
509 Interface Sci.* **2008**, *320* (2), 400–414. <https://doi.org/10.1016/j.jcis.2008.01.007>.
- 510 (28) Boily, J.-F.; Persson, P.; Sjöberg, S. Benzenecarboxylate Surface Complexation at the Goethite  
511 ( $\alpha$ -FeOOH)/Water Interface: II. Linking IR Spectroscopic Observations to Mechanistic Surface  
512 Complexation Models for Phthalate, Trimellitate, and Pyromellitate. *Geochim. Cosmochim.  
513 Acta* **2000**, *64* (20), 3453–3470.
- 514 (29) Boily, J.-F.; Kozin, P. A. Particle Morphological and Roughness Controls on Mineral Surface  
515 Charge Development. *Geochim. Cosmochim. Acta* **2014**, *141*, 567–578.  
516 <https://doi.org/10.1016/j.gca.2014.06.016>.
- 517 (30) Rietra, R. P. J. J.; Hiemstra, T.; van Riemsdijk, W. H. Comparison of Selenate and Sulfate  
518 Adsorption on Goethite. *J. Colloid Interface Sci.* **2001**, *240* (2), 384–390.  
519 <https://doi.org/10.1006/jcis.2001.7650>.
- 520 (31) Fukushi, K.; Sverjensky, D. A. A Surface Complexation Model for Sulfate and Selenate on  
521 Iron Oxides Consistent with Spectroscopic and Theoretical Molecular Evidence. *Geochim.  
522 Cosmochim. Acta* **2007**, *71* (1), 1–24. <https://doi.org/10.1016/j.gca.2006.08.048>.
- 523 (32) Hinkle, M. A. G.; Wang, Z.; Giammar, D. E.; Catalano, J. G. Interaction of Fe(II) with  
524 Phosphate and Sulfate on Iron Oxide Surfaces. *Geochim. Cosmochim. Acta* **2015**, *158*, 130–146.  
525 <https://doi.org/10.1016/j.gca.2015.02.030>.
- 526 (33) Johnston, C. P.; Chrysochoou, M. Mechanisms of Chromate, Selenate, and Sulfate Adsorption  
527 on Al-Substituted Ferrihydrite: Implications for Ferrihydrite Surface Structure and Reactivity.  
528 *Environ. Sci. Technol.* **2016**, *50* (7), 3589–3596. <https://doi.org/10.1021/acs.est.5b05529>.
- 529 (34) Boukhalfa, C. Sulfate Removal from Aqueous Solutions by Hydrous Iron Oxide in the  
530 Presence of Heavy Metals and Competitive Anions. *Desalination* **2010**, *250* (1), 428–432.  
531 <https://doi.org/10.1016/j.desal.2009.09.070>.
- 532 (35) Peak, D.; Ford, R. G.; Sparks, D. L. An in Situ ATR-FTIR Investigation of Sulfate Bonding  
533 Mechanisms on Goethite. *J. Colloid Interface Sci.* **1999**, *218* (1), 289–299.  
534 <https://doi.org/10.1006/jcis.1999.6405>.
- 535 (36) Wijnja, H.; Schulthess, C. P. Vibrational Spectroscopy Study of Selenate and Sulfate  
536 Adsorption Mechanisms on Fe and Al (Hydr)Oxide Surfaces. *J. Colloid Interface Sci.* **2000**,  
537 *229* (1), 286–297. <https://doi.org/10.1006/jcis.2000.6960>.
- 538 (37) Rahnamaie, R.; Hiemstra, T.; van Riemsdijk, W. H. Inner- and Outer-Sphere Complexation of  
539 Ions at the Goethite–Solution Interface. *J. Colloid Interface Sci.* **2006**, *297* (2), 379–388.  
540 <https://doi.org/10.1016/j.jcis.2005.11.003>.
- 541 (38) Weng, L.; Van Riemsdijk, W. H.; Hiemstra, T. Cu<sup>2+</sup> and Ca<sup>2+</sup> adsorption to Goethite in the  
542 Presence of Fulvic Acids. *Geochim. Cosmochim. Acta* **2008**, *72* (24), 5857–5870.  
543 <https://doi.org/10.1016/j.gca.2008.09.015>.
- 544 (39) Gu, X.; Tan, Y.; Tong, F.; Gu, C. Surface Complexation Modeling of Coadsorption of  
545 Antibiotic Ciprofloxacin and Cu(II) and onto Goethite Surfaces. *Chem. Eng. J.* **2015**, *269*, 113–  
546 120. <https://doi.org/10.1016/j.cej.2014.12.114>.

- 547 (40) Guaita, D. P.; Sayen, S.; Boudesocque, S.; Guillon, E. Copper(II) Influence on Flumequine  
548 Retention in Soils: Macroscopic and Molecular Investigations. *J. Colloid Interface Sci.* **2011**,  
549 *357* (2), 453–459. <https://doi.org/10.1016/j.jcis.2011.01.097>.
- 550 (41) Ali, M. A.; Dzombak, D. A. Effects of Simple Organic Acids on Sorption of Cu<sup>2+</sup> and Ca<sup>2+</sup>  
551 on Goethite. *Geochim. Cosmochim. Acta* **1996**, *60* (2), 291–304.
- 552 (42) Fein, J. B. The Effects of Ternary Surface Complexes on the Adsorption of Metal Cations and  
553 Organic Acids onto Mineral Surfaces. In: R. Hellmann and S.A. Wood (Editors), *Water-Rock*  
554 *Interactions, Ore Deposits, and Environmental Geochemistry: A Tribute to David A. Crerar*.  
555 *Geochemical Society, Special Pub. 7*, pp. 365–378.
- 556 (43) Swedlund, P. J.; Webster, J. G.; Miskelly, G. M. Goethite Adsorption of Cu(II), Pb(II), Cd(II),  
557 and Zn(II) in the Presence of Sulfate: Properties of the Ternary Complex. *Geochim.*  
558 *Cosmochim. Acta* **2009**, *73* (6), 1548–1562. <https://doi.org/10.1016/j.gca.2008.12.007>.
- 559 (44) Hiemstra, T.; Van Riemsdijk, W. H. Fluoride Adsorption on Goethite in Relation to Different  
560 Types of Surface Sites. *J. Colloid Interface Sci.* **2000**, *225* (1), 94–104.  
561 <https://doi.org/10.1006/jcis.1999.6697>.
- 562 (45) Porro, I.; Newman, M. E.; Dunnivant, F. M. Comparison of Batch and Column Methods for  
563 Determining Strontium Distribution Coefficients for Unsaturated Transport in Basalt. *Environ.*  
564 *Sci. Technol.* **2000**, *34* (9), 1679–1686. <https://doi.org/10.1021/es9901361>.
- 565 (46) Altfelder, S.; Streck, T.; Maraqa, M. A.; Voice, T. C. Nonequilibrium Sorption of  
566 Dimethylphthalate—Compatibility of Batch and Column Techniques. *Soil Sci. Soc. Am. J.*  
567 **2001**, *65* (1), 102–111. <https://doi.org/10.2136/sssaj2001.651102x>.
- 568 (47) Hanna, K.; Lassabatere, L.; Bechet, B. Transport of Two Naphthoic Acids and Salicylic Acid in  
569 Soil: Experimental Study and Empirical Modeling. *Water Res.* **2012**, *46* (14), 4457–4467.  
570 <https://doi.org/10.1016/j.watres.2012.04.037>.
- 571 (48) Hanna, K.; Rusch, B.; Lassabatere, L.; Hofmann, A.; Humbert, B. Reactive Transport of  
572 Gentisic Acid in a Hematite-Coated Sand Column: Experimental Study and Modeling.  
573 *Geochim. Cosmochim. Acta* **2010**, *74* (12), 3351–3366.  
574 <https://doi.org/10.1016/j.gca.2010.03.022>.
- 575 (49) Rahnemaie, R.; Hiemstra, T.; van Riemsdijk, W. H. Carbonate Adsorption on Goethite in  
576 Competition with Phosphate. *J. Colloid Interface Sci.* **2007**, *315* (2), 415–425.  
577 <https://doi.org/10.1016/j.jcis.2007.07.017>.

578

579

580 **Table 1. Surface Complexation Model**

581

<b>Aqueous solutions</b>	<b>log K</b>	<b>b<sub>i</sub></b>			<b>ref.</b>
$\text{OAH}_{(s)} \rightleftharpoons \text{OAH}_{(aq)}$	-5.06	0			8
$\text{OA}^- + \text{H}^+ \rightleftharpoons \text{OAH}$	6.92	0			8
$\text{OA}^- + \text{Mg}^{+2} \rightleftharpoons \text{OAMg}^+$	3.51	0.5±0.1			10
$\text{OA}^- + \text{Cu}^{+2} \rightleftharpoons \text{OACu}^+$	6.61	0.5( $b_{\text{OAMg}^+}$ )			10
$\text{OA}^- + \text{Ca}^{+2} \rightleftharpoons \text{OACa}^+$	2.61	0.5( $b_{\text{OAMg}^+}$ )			10
<b>Surface reactions</b>	<b>log K</b>	<b>Δz<sub>0</sub></b>	<b>Δz<sub>1</sub></b>	<b>Δz<sub>2</sub></b>	
$\equiv\text{Fe}_3\text{O}^{-0.5} + \text{H}^+ \rightleftharpoons \equiv\text{Fe}_3\text{OH}^{+0.5}$	9.1	+1	0	0	8
$\equiv\text{Fe}_3\text{O}^{-0.5} + \text{H}^+ + \text{Cl}^- \rightleftharpoons \equiv\text{Fe}_3\text{OH}_2^{+0.5}\cdots\text{Cl}^-$	8.1	+1	0	-1	8
$\equiv\text{Fe}_3\text{O}^{-0.5} + \text{Na}^+ \rightleftharpoons \equiv\text{Fe}_3\text{OH}^{-0.5}\cdots\text{Na}^+$	-1	0	0	+1	8
$\equiv\text{FeOH}^{-0.5} + \text{H}^+ \rightleftharpoons \equiv\text{FeOH}_2^{+0.5}$	9.1	+1	0	0	8
$\equiv\text{FeOH}^{-0.5} + \text{H}^+ + \text{Cl}^- \rightleftharpoons \equiv\text{FeOH}_2^{+0.5}\cdots\text{Cl}^-$	8.1	+1	0	-1	8
$\equiv\text{FeOH}^{-0.5} + \text{Na}^+ \rightleftharpoons \equiv\text{FeOH}^{-0.5}\cdots\text{Na}^+$	-1	0	0	+1	8
$2 \text{H}^+ + 2 \equiv\text{FeOH}^{-0.5} + \text{OA}^- \rightleftharpoons (\equiv\text{Fe})_2(\text{OA})^0 + 2 \text{H}_2\text{O}$	20.6±0.1	+1	0	0	8
$2 \text{H}^+ + 2 \equiv\text{FeOH}^{-0.5} + \text{OA}^- \rightleftharpoons (\equiv\text{FeOH}_2)_2^+ \cdots \text{OA}^-$	20.6±0.1	+1.6	-0.6	0	8
$2 \equiv\text{FeOH}^{-0.5} + \text{Mg}^{+2} \rightleftharpoons (\equiv\text{FeOH})_2\text{Mg}^+$	4.89	+0.71	+1.29	0	30
$2 \equiv\text{FeOH}^{-0.5} + \text{Mg}^{+2} + \text{H}_2\text{O} \rightleftharpoons (\equiv\text{FeOH})_2\text{MgOH} + \text{H}^+$	-6.44	+0.71	+0.29	0	30
$\equiv\text{FeOH}^{-0.5} + \text{Ca}^{+2} \rightleftharpoons \equiv\text{FeOHCa}^{+1.5}$	2.85	0	+2	0	30
$\equiv\text{Fe}_3\text{O}^{-0.5} + \text{Ca}^{+2} \rightleftharpoons \equiv\text{Fe}_3\text{OCA}^{+1.5}$	2.85	0	+2	0	30
$\equiv\text{FeOH}^{-0.5} + \text{Ca}^{+2} \rightleftharpoons \equiv\text{FeOHCa}^{+1.5}$	3.69	+0.32	+1.68	0	30
$\equiv\text{FeOH}^{-0.5} + \text{Ca}^{+2} + \text{H}_2\text{O} \rightleftharpoons \equiv\text{FeOHCaOH}^{+1.5} + \text{H}^+$	-9.17	+0.32	+0.68	0	30
$\text{H}^+ + \equiv\text{FeOH}^{-0.5} + \text{SO}_4^{-2} \rightleftharpoons (\equiv\text{Fe})(\text{SO}_4)^{1.5-} + \text{H}_2\text{O}$	8.0±0.2*(9.37)	+0.5	-1.5	0	37
$\text{H}^+ + \equiv\text{FeOH}^{-0.5} + \text{SO}_4^{-2} \rightleftharpoons (\equiv\text{Fe})(\text{SO}_4)^{1.5-} \cdots \text{H}_2\text{O}$	9.7±0.2*(11.06)	+1	-1.84	-0.16	37
$2 \equiv\text{FeOH}^{-0.5} + \text{Cu}^{+2} \rightleftharpoons (\equiv\text{FeOH})_2\text{Cu}^+$	9.18	+0.84	+1.16	0	38
$2 \equiv\text{FeOH}^{-0.5} + \text{Cu}^{+2} + \text{H}_2\text{O} \rightleftharpoons (\equiv\text{FeOH})_2\text{CuOH} + \text{H}^+$	4.6±0.1*(3.6)	+0.84	+0.16	0	38
$2 \equiv\text{FeOH}^{-0.5} + 2 \text{Cu}^{+2} + 2 \text{H}_2\text{O} \rightleftharpoons (\equiv\text{FeOH})_2\text{Cu}_2(\text{OH})_2^+ + 2 \text{H}^+$	3.65	+0.84	+1.16	0	38
$2 \equiv\text{FeOH}^{-0.5} + 2 \text{Cu}^{+2} + 3 \text{H}_2\text{O} \rightleftharpoons (\equiv\text{FeOH})_2\text{Cu}_2(\text{OH})_3 + 3 \text{H}^+$	-3.1	+0.84	+0.16	0	38
$2 \equiv\text{FeOH}^{-0.5} + \text{OA}^- + \text{Cu}^{+2} \rightleftharpoons (\equiv\text{FeOH})_2\text{CuOA}$	18±0.1	+1.3	-0.3	0	P.W.
$2 \equiv\text{FeOH}^{-0.5} + \text{Cu}^{+2} + \text{SO}_4^{-2} \rightleftharpoons (\equiv\text{FeOH})_2\text{CuSO}_4^-$	12.6±0.2	+1.5	-1.5	0	P.W.
$\equiv\text{FeOH}^{-0.5} + \text{H}^+ + \text{F}^- \rightleftharpoons \equiv\text{FeF}^{-0.5} + \text{H}_2\text{O}$	9.6	+0.4	-0.4	0	44
$2 \text{H}^+ + 2 \equiv\text{FeOH}^{-0.5} + \text{CO}_3^{-2} \rightleftharpoons (\equiv\text{Fe})_2(\text{CO}_3)^{-1} + 2 \text{H}_2\text{O}$	22.01	+0.62	-0.62	0	49
$2 \text{H}^+ + 2 \equiv\text{FeOH}^{-0.5} + \text{CO}_3^{-2} + \text{Na}^+ \rightleftharpoons (\equiv\text{Fe})_2(\text{CO}_3\text{Na})^0 + 2 \text{H}_2\text{O}$	22.03	+0.62	+0.38	0	49
$\text{H}^+ + \equiv\text{FeOH}^{-0.5} + \text{CO}_3^{-2} \rightleftharpoons \equiv\text{FeOH}_2\text{CO}_3^{-1.5}$	10.22	+1	-2	0	49
$\text{H}^+ + \equiv\text{Fe}_3\text{O}^{-0.5} + \text{CO}_3^{-2} \rightleftharpoons \equiv\text{Fe}_3\text{OHCO}_3^{-1.5}$	10.22	+1	-2	0	49

582 \*adjusted from the original work. Log K values are given at I = 0. Parameter “b<sub>i</sub>” is used in the

583 WATEQ equation. The original constants from literature are in the brackets.

584

